ABSTRACT

LaPointe, Stephen James. Growth of binary alloyed semiconductor crystals by the vertical Bridgman-Stockbarger process with a strong magnetic field. (Under the direction of Dr. Nancy Ma.)

This thesis presents a model for the unsteady species transport for the growth of alloyed semiconductor crystals during the vertical Bridgman-Stockbarger process with a steady axial magnetic field. During growth of alloyed semiconductors such as germanium-silicon (GeSi) and mercury-cadmium-telluride (HgCdTe), the solute's concentration is not small so that density differences in the melt are very large. These compositional variations drive compositionally-driven buoyant convection, or solutal convection, in addition to thermally-driven buoyant convection. These buoyant convections drive convective transport which produces non-uniformities in the concentration in both the melt and the crystal. This transient model predicts the distribution of species in the entire crystal grown in a steady axial magnetic field. The present study presents results of concentration in the crystal and in the melt at several different stages during crystal growth.

Growth of binary alloyed semiconductor crystals by the vertical Bridgman-Stockbarger process with a strong magnetic field

by

Stephen James LaPointe

A thesis submitted to the Graduate Faculty of
North Carolina State University
in partial fulfillment of the
requirements for the degree of
Master of Science

Department of Mechanical and Aerospace Engineering

Raleigh

2004

Approved By:

Dr. K. M. Lyons, Member	Dr. R. R. Johnson, Member

Dr. N. Ma, Chair

Biography

Stephen LaPointe was born in Schenectady, New York on June 2, 1981. Raised in Scotia, New York, he graduated from Burnt Hills-Ballston Lake High School in 1999. Wishing to further his education, he enrolled in the mechanical engineering department of North Carolina State University, where he received his Bachelor's Degree in Mechanical Engineering in 2003. He continued his education at North Carolina State University to earn his Master's Degree in Mechanical Engineering in 2004.

Acknowledgements

I would like to start out by thanking Dr. Kevin Lyons and Dr. Richard Johnson for taking the time to be on my committee. I would also like to thank the National Aeronautics and Space Administration for funding this work.

I am indebted to my advisor, Dr. Nancy Ma, for giving the opportunity to work with her. Her knowledge and advice proved invaluable during this project and allowed me to enjoy my work. I thank her for her support.

I would like to say thanks to all of my friends and family who have supported and encouraged me in many different ways during my time at North Carolina State University. Lastly, a very special thank you to Sandra, without whom I would not have been able to accomplish any of this. Her support has been instrumental in my successes.

Table Of Contents

List Of Figures

Page

List Of Symbols

a	initial dimensionless melt depth
b	dimensionless melt depth
B	magnetic flux density
Bi	Biot number for the heat transfer from the furnace through the ampoule wall
C	dimensionless concentration in the melt
C*	concentration or mole fraction of solute in the melt
C_o	initial uniform mole fraction of the solute in the melt
c_p	specific heat of the melt
d	dimensionless vertical distance between the crystal-melt interface and the vertical position where the adiabatic and hot-zone meet
D	diffusion coefficient for the solute in the molten semiconductor
g	gravitational acceleration
Ha	Hartmann number
I_0	modified Bessel function of the first kind and zeroth order
I_1	modified Bessel function of the first kind and first order
k	thermal conductivity of the melt
k_s	segregation coefficient for silicon in germanium
n	summation index
N	interaction parameter
$\hat{\mathbf{n}}$	unit normal vector
Pe_g	growth Péclet number
Pe_m	species transport Péclet number
Pe_t	thermal Péclet number
r	dimensionless radial coordinate in the melt
$\hat{\mathbf{r}}$	unit vector in the radial direction

R radius of the crystal

R_m magnetic Reynolds number

t dimensionless time

T dimensionless temperature in the melt

T^* temperature in the melt

T_o solidification temperature

U characteristic velocity for the magnetically-damped solutal convection

U_g growth rate or velocity of the crystal-melt interface

v dimensionless velocity in the melt

v_r dimensionless radial velocity in the melt

v_z dimensionless axial velocity in the melt

z dimensionless axial coordinate in the melt

$\hat{\mathbf{z}}$ unit vector in the axial direction

Greek Symbols

$(\Delta C)_o$ characteristic mole fraction variation

$(\Delta T)_o$ difference between the hot-zone temperature and the solidification temperature

β_C compositional coefficient of volumetric expansion

β_T thermal coefficient of volumetric expansion

γ characteristic ratio of thermally-driven buoyant convection to compositionally-driven buoyant (solutal) convection

ζ dimensionless rescaled axial coordinate in the melt

θ dimensionless azimuthal coordinate in the melt

$\hat{\boldsymbol{\theta}}$ unit vector in the azimuthal direction

μ_p magnetic permeability of the melt

μ dynamic viscosity of the melt

π 3.14159 radians

ρ density of the melt

ρ_o density of the melt at the solidification temperature

σ electrical conductivity of the melt

ϕ dimensionless electric potential function

ψ dimensionless streamfunction in the melt

ω dimensionless interface velocity

χ coefficient in the separation-of-variables solution for temperature

1. Introduction

1.1 Effects of a Magnetic Field

During crystal growth without a magnetic field or with a weak magnetic field, turbulent or oscillatory melt motions can produce undesirable spatial oscillations of the concentration, or microsegregation, in the crystal [1]. Turbulent or oscillatory melt motions lead to fluctuations in the heat transfer across the growth interface from the melt to the crystal. Since the local rate of crystallization depends on the balance between the local heat fluxes in the melt and the crystal, fluctuations in the heat flux from the melt create fluctuations in the local growth rate which create microsegregation. A moderate magnetic field can be used to create a body force which provides an electromagnetic (EM) damping of the melt motion and to eliminate oscillations in the melt motion and thus in the concentration of the crystal. Unfortunately, the elimination of mixing and a moderate or strong EM damping of the residual melt motion may lead to a large variation of the crystal's composition in the direction perpendicular to the growth direction (radial macrosegregation).

On the other hand, if the magnetic field strength is so strong that the melt motion is reduced sufficiently so that it has no effect on the composition in the crystal, then this diffusion-controlled species transport may produce a radially and axially uniform composition in the crystal grown by the Bridgman-Stockbarger process of directional solidification [2]. In order to achieve diffusion-controlled species transport, the species transport Péclet number Pe_m=UR/D must be small, where U is

the characteristic velocity for the magnetically-damped melt motion and is inversely proportional to the square of the magnetic flux density B, while R is the characteristic dimension of the melt and D is the diffusion coefficient for the species in the molten semiconductor. If $Pe_m<<1$, then the characteristic ratio of convection to diffusion of species is small and the species transport is diffusion controlled. However, since typical values of D are extremely small [3], i.e. 1 to $2x10^{-8}$ m^2/s, it would not be practical to grow a crystal in the extremely large field strength that would be required to achieve diffusion-controlled species transport. Even for the strongest magnetic fields available with superconducting magnets , $Pe_m>1$. As the magnetic field strength decreases, the value of Pe_m increases. Therefore the objective is to identify a magnetic field which is strong enough to eliminate flow oscillations but which moderately damps the melt motion in order to improve both radial and axial uniformity in the crystal.

For alloyed semiconductor crystal growth, the density differences due to compositional variations in the melt are very large. During the growth of alloyed semiconductor crystals such as silicon-germanium (GeSi) or mercury-cadmium-telluride (HgCdTe), both compositional and thermal variations in the melt create density differences which drive solutal convection. This solutal convection drives species transport which causes segregation in the crystal. In germanium-silicon, for example, the mole fraction of germanium may vary from 0.95 in the melt which has not yet received any rejected germanium to 0.99 near the interface, and this

compositional difference corresponds to a density difference of nearly 300 kg/m^3. During growth of alloyed semiconductor crystals, the application of magnetic fields have shown great promise. For example, Watring and Lehoczky [4] have shown that the radial variation between the maximum and minimum concentrations can be decreased by more than a factor of three with the application of a 5 T magnetic field, arising because the magnetic field retards the sinking of the heavier melt to the center of the ampoule which results in less radial segregation. Ramachandran and Watring [5] reported a reduction in the radial segregation in all of their samples which were grown in a magnetic field Alboussiere *et al*. [6] also experimentally investigated the influence of a magnetic field on segregation in a metallic alloy.

For a typical crystal growth process, resolution of thin species-diffusion boundary layers having an $O(Pe_m^{-1})$ thickness is often very challenging because the species transport Péclet number can have very large values. Several grid points must be concentrated inside each layer in order to give accurate results because these boundary layers play critical roles in the transport. As the magnetic flux density B of the externally-applied magnetic field is increased, the value of Pe_m decreases and the species-diffusion boundary layers become thicker, but the value of the Hartmann number $Ha=BR(\sigma/\mu)^{1/2}$ increases, where σ and μ are the electrical conductivity and dynamic viscosity of the melt, respectively. Therefore, there are thin species-diffusion or viscous boundary layers for every value of B. Therefore the simultaneous numerical solution of the full Navier-Stokes, internal energy and

species transport must always have a very fine spatial grid and a very small time step. Models which accurately predict the species distribution in an entire crystal for any combination of process variables are needed to facilitate process optimization.

In a previous study [7], we presented an asymptotic and numerical solution for the dilute species transport during the solidification of a doped crystal by the Bridgman-Stockbarger process with a steady axial magnetic field. This study only considered pure crystals with very small dopant concentrations so that there was only thermally-driven buoyant convection. During the growth of alloyed semiconductor crystals, the velocity and mole fraction of either species are intrinsically coupled because the buoyant convection is driven by both the thermal and compositional variations in the melt. In the 1970s, Hart [8] presented an asymptotic and numerical solution for the motion of a stratified salt solution with both thermally-driven and compositionally-driven buoyant convection, or solutal convection, and without a magnetic field or solidification in a rectangular cavity. Ma [9] and Farrell and Ma [10] presented an asymptotic and numerical solution for the motion of a molten semiconductor with solutal convection, with a magnetic field and with solidification in a rectangular cavity. Liu *et al*. [11] numerically studied solutal convection during the traveling heater method with a magnetic field. Several important studies [12-15] have numerically investigated the effects of solutal convection on segregation during solidification without magnetic fields. In the

present study, we treat the species transport during the solidification of a germanium-silicon alloy during a realistic process, namely, the vertical Bridgman-Stockbarger process with a uniform, steady, axial magnetic field. The present study eliminates the need for impractical computing resources by using an asymptotic approach to treat the entire period of time needed to grow a crystal. This approach involves an analytic solution to the internal energy equation, and a hybrid solution for the simplified coupled Navier-Stokes, electromagnetic and species transport equations. The purpose of this paper is to illustrate a method which can be used to optimize the benefits of a magnetic field for a given crystal growth situation.

Researchers have reviewed the literature on crystal growth in the presence of magnetic fields. Garandet and Alboussière [16] reviewed the literature on experimental studies of Bridgman-Stockbarger growth of semiconductor crystals, and Walker [17] reviewed the use of asymptotic methods in modelling of semiconductor crystal growth.

2. Temperature

This paper treats the unsteady, axisymmetric species transport of silicon in a germanium melt during the vertical Bridgman-Stockbarger process with an externally applied, uniform, steady, axial magnetic field $B\hat{\mathbf{z}}$. Here, $\hat{\mathbf{r}}$, $\hat{\boldsymbol{\theta}}$ and $\hat{\mathbf{z}}$ are the unit vectors for the cylindrical coordinate system. During the Bridgman-Stockbarger process, the ampoule is moved from an isothermal hot zone where the

germanium-silicon has been melted, through an adiabatic or thermal-gradient zone where the melt solidifies, and into a cold zone where the crystal is cooled. Our dimensionless problem is sketched in Fig. 1. The coordinates and lengths are normalized by the ampoule's inner radius R, and a is the dimensionless length of the ampoule.

Experiments [4] have shown that magnetic fields can control compositionally-driven buoyant convection so that the electromagnetic body force must be comparable to the characteristic gravitational body force associated with compositional variations. Since the electric currents only arise from the melt motions across the magnetic field, the magnetic field can damp the melt motion but cannot completely suppress it. Therefore, this balance gives a characteristic velocity for the magnetically-damped compositionally-driven buoyant or solutal convection [9],

$$U = \frac{\rho_o g \beta_c C_o}{\sigma B^2} , \tag{1}$$

where ρ_o is the melt's density at the solidification temperature T_o, g is gravitational acceleration, β_c is the compositional coefficient of volumetric expansion, and C_o is the initial uniform mole fraction of silicon in germanium. Thus, we can expect the melt motion to decrease roughly as B^{-2} as the magnetic field strength is increased.

The crystal-melt interface moves at a constant velocity $U_g=\omega U$, where ω is the dimensionless interface velocity. The planar crystal-melt interface lies at z=-b, where the instantaneous dimensionless axial length $b(t)=a-\omega t$ decreases during growth. With time t normalized by R/U, the dimensionless time to grow the entire crystal is a/ω.

The characteristic ratio of the convective to conductive heat transfer is the thermal Péclet number $Pe_t=\rho_o^2 g\beta_c C_o c_p R/k\sigma B^2$, which varies as B^{-2}. Here, c_p and k are the specific heat and the thermal conductivity of the melt, respectively. For a sufficiently large value of B and for practical growth rates, convective heat transfer and the heat released by the cooling melt are negligible compared to the conductive heat transfer [18]. Ma and Walker [19] investigated the effects of convective heat transfer on the temperature distribution and on the thermally-driven buoyant convection are negligible for $Pe_t<15.0$. For molten germanium-silicon with R=7.5 mm, B=0.5 T and $C_o=0.10$, $Pe_t=3.44$. This value of Pe_t is sufficiently small that convective heat transfer is negligible.

As long as the furnace is axisymmetric, the melt's temperature is independent of θ, and $T(r,\zeta)$ is the deviation of the melt's dimensional temperature from the hot-zone temperature, normalized by $(\Delta T)_o$ where $(\Delta T)_o$ is the difference between the hot-zone temperature and T_o. Here, $\zeta=1+2z/b$ is a rescaled axial coordinate, so that $-1\le\zeta\le+1$ for all time. For each instantaneous melt depth, the temperature is given by a separation-of-variables solution [7],

$$T = \frac{1}{2}(\zeta - 1) + \sum_{n=1}^{\infty} \chi_n I_o\left(\frac{n\pi r}{b}\right) \sin\left[\frac{n\pi}{2}(\zeta - 1)\right], \tag{2a}$$

$$\chi_n = \frac{\frac{2b}{dn^2\pi^2} \sin\left[\frac{n\pi}{b}(-b + d)\right]}{\frac{n\pi}{bBi} I_1\left(\frac{n\pi}{b}\right) + I_0\left(\frac{n\pi}{b}\right)}, \tag{2b}$$

where I_0 or I_1 is the modified Bessel function of the first kind and zeroth or first order. Here, d is the dimensionless vertical distance between the crystal-melt interface and the vertical position where the adiabatic and hot-zone meet, while Bi is the Biot number for the heat transfer from the furnace through the ampoule wall. Some typical isotherms for Bi=10, d=0.1, and b=1.0 are presented in Fig. 2. The thermal gradients are concentrated in a region of the melt near the crystal-melt interface because this region of the ampoule is adjacent to the furnace's thermal-gradient zone. The remainder of the melt, which lies adjacent to the hot-zone is isothermal at the hot-zone temperature.

The model is idealized because we have assumed that the crystal-melt interface is planar. The heat flux is primarily axial in the thermal-gradient zone where the crystal-melt interface lies. Since the thermal conductivity of the solid germanium is less than half that of the melt, the crystal represents a thermal barrier causing some of the heat flux to flow radially outward to the ampoule wall near the interface. This

local radial heat flux causes the local isotherms and the crystal-melt interface to be concave into the crystal [5]. Future research will investigate the effect of the curved crystal-melt interface on the solutal convection.

3. Solutal Convection

We assume that the temperature differences and compositional variations are sufficiently small that all the thermophysical properties of the melt can be considered uniform and constant except for the density in the gravitational body force term of the momentum equation. In this Boussinesq-like approximation, the characteristic temperature difference $(\Delta T)_o$ and characteristic mole fraction variation $(\Delta C)_o$ are assumed to be sufficiently small that the melt's density is a linear function of temperature and composition, given by

$$\rho = \rho_o \left[1-\beta_T(T^*-T_o)-\beta_c(C^*-C_o)\right] , \tag{3}$$

and that $\beta_T(\Delta T)_o<<1$ and $\beta_c(\Delta C)_o<<1$, where T^* is the temperature in the melt, C^* is the mole fraction of one species in the melt, and C_o is the initially uniform mole fraction in the melt before crystal growth begins.

The electric current in the melt produces an induced magnetic field, which is superimposed on the applied magnetic field produced by the external magnet. The

characteristic ratio of the induced to the applied magnetic field strengths is the magnetic Reynolds number,

$$R_m=\mu_p\sigma UR\,, \tag{4}$$

where μ_p is the magnetic permeability of the melt. For all crystal-growth processes, $R_m<<1$ and the additional magnetic fields produced by the electric currents in the melt are negligible.

In the Navier-Stokes equation, the characteristic ratio of the EM body force term to the inertial terms is the interaction parameter $N=\sigma^2B^4R/\rho_o^2g\beta_cC_o$, which varies at B^4. Ma and Walker [19] investigated the role of inertia on the thermally-driven buoyant convection during crystal growth and determined the errors associated with the neglect of inertial effects for interaction parameters between between N=1.307 and N=6,803.5. We found that inertia significantly affects the buoyant convection for which N=1.037. As the interaction parameter is increased from this value, so that the ratios of the inertial force to the EM body force decrease. We found that the error due to neglect of inertial effects is only 2.7% for N=16.59. For molten germanium-silicon with R=7.5 mm, B=0.5 T and C_o=0.10, N=57.3. This value of N is sufficiently small that inertial effects are negligible.

In an asymptotic solution for Ha>>1, the melt is divided into an inviscid core, Hartmann layers with $O(Ha^{-1})$ thickness adjacent to the boundaries at $\zeta=\pm1$, and a

parallel layer with an $O(Ha^{-1/2})$ thickness adjacent to the ampoule surface at r=1. The Hartmann layers have a simple, local, exponential structure, which matches any radial core or parallel-layer velocities at $\zeta=\pm1$, which satisfies the no-slip conditions at the solid-liquid interface and at the surface of the ampoule, and which indicates that v_z in the core or parallel layer is $O(Ha^{-1})$ at $\zeta=\pm1$. Analysis of the parallel layer reveals that its thickness is actually $O[(b/Ha)^{1/2}]$ while the axial velocity is $O[(Ha/b)^{1/2}]$. Since b can be as large as 35 at the beginning of the Bridgman-Stockbarger process, the parallel layer is not actually thin as assumed in the formal asymptotic expansion for Ha>>1. While a formal asymptotic analysis for Ha>>1 is not appropriate, the numerical solution of the inertialess Navier-Stokes equation with all viscous terms is not necessary. The Hartmann layers represent an extremely small fraction of the melt length and have a simple exponential structure. There is no need to numerically duplicate this simple exponential structure. Therefore, we use a composite core-parallel-layer solution which does not assume that the parallel-layer thickness is small. We discard the viscous terms $Ha^{-2}\partial^2\mathbf{v}/\partial z^2$ in the Navier-Stokes equation, we relax the no-slip conditions at $\zeta=\pm1$ because they are satisfied by the Hartmann layers which are not part of the composite solution, and we apply the boundary conditions

$$v_z=0 \text{ , at } \zeta=\pm1 \text{ .} \qquad (5)$$

Here, $\mathbf{v}=v_r\hat{\mathbf{r}}+v_z\hat{\mathbf{z}}$ is the velocity normalized by U where $\hat{\mathbf{r}}$ and $\hat{\mathbf{z}}$ are the unit vectors for the cylindrical coordinate system. Since these conditions neglect the $O(Ha^{-1})$ perturbation velocity due to the Hartmann layers, we also discard the other viscous terms in the radial component of the Navier-Stokes equation because they are $O(Ha^{-1})$ compared to the radial pressure gradient in both the core and the parallel layer, and we already have an $O(Ha^{-1})$ error. There are $O(Pe_m^{-1})$ species-diffusion boundary layers adjacent to the crystal-melt interface and adjacent to the surfaces of the ampoule. Matching the solutions for C in the Hartmann layers, the boundary conditions at the crystal-melt interface and at the top of the ampoule are

$$\frac{2}{b}\frac{\partial C}{\partial \zeta} = Pe_g\,(k_s - 1)\,C \quad , \quad \text{at } \zeta=-1 \, , \tag{6a}$$

$$\frac{\partial C}{\partial \zeta} = 0 \quad , \quad \text{at } \zeta=+1 \, , \tag{6b}$$

where $Pe_g=U_gR/D=\omega Pe_m$ is the growth Péclet number and k_s is the segregation coefficient.

Therefore the dimensionless equations governing the composite core-parallel-layer solution, which assumes that the Hartmann layers have negligible thickness and which has an $O(Ha^{-1})$ relative error, are

$$Ha^{-2}\left(\frac{\partial^4\psi}{\partial r^4}-\frac{2}{r}\frac{\partial^3\psi}{\partial r^3}+\frac{3}{r^2}\frac{\partial^2\psi}{\partial r^2}-\frac{3}{r^3}\frac{\partial\psi}{\partial r}\right)-\frac{4}{b^2}\frac{\partial^2\psi}{\partial\zeta^2}=\gamma\, r\frac{\partial T}{\partial r}+r\frac{\partial C}{\partial r}, \tag{7a}$$

$$\gamma=\frac{\beta_T(\Delta T)_o}{\beta_c C_o}, \tag{7b}$$

$$\frac{\partial C}{\partial t}+\mathbf{v}\bullet\nabla C=Pe_m^{-1}\nabla^2 C, \tag{7c}$$

where C is the mole fraction of silicon in the germanium-silicon mixture normalized by the initial uniform mole fraction C_o. The boundary conditions along the impermeable surfaces of the ampoule are $\hat{\mathbf{n}}\bullet\nabla C=0$.

We use a Chebyshev spectral collocation method in order to solve Eqs. (7a) and (7c) with Gauss-Lobatto collocation points in r and ζ. We use a sufficient number of collocation points in order to resolve the large velocity and concentration gradients near r=1. All values of B require a significant number of collocation points since Ha is proportional to B, while Pe_m is proportional to B^{-2}. For the time derivative in Eq. (7c), we use a second-order implicit time integration scheme to integrate from t=0 to a time which is slightly less than a/ω. We chose a large enough number of time steps so that the results are not changed by increasing the number of time steps. We found that 41 collocation points in the radial direction, 41 collocation points in the axial direction and 12,800 time steps were enough to resolve the velocity and

concentration gradients in the melt. Further increasing these numbers did not change the results.

At the beginning of crystal growth, the melt concentration, normalized by the initial uniform concentration, is $C(r,\zeta,t=0)=1$. Thus, the amount of solute initially in the melt is obtained by integrating across the ampoule's volume giving a total solute concentration equal to πa. We verify that the sum of the total solute in the melt and in the crystal is equal to πa at each time step.

Assuming that there is no diffusion of solute in the solid crystal, the solute distribution in the crystal, $C_s(r,z)$, normalized by the initial uniform solute concentration in the melt, is given by

$$C_s(r, z) = k_s C\left(r, \zeta=-1, t=\frac{z}{\omega}\right), \tag{8}$$

where $k_s=4.2$ for silicon in a germanium melt.

4. Results

We present results for B=0.5 T, $C_o=0.10$ and $U_g=23$ μm/s, for which U=0.008334 m/s, Ha=165.9, $Pe_m=3{,}125$, $Pe_g=8.625$, $\gamma=0.09246$ and $\omega=0.00276$. For a=1, the dimensionless time to grow a crystal is $a/\omega=362.3$.

Initially at t=0, the concentration in the melt is uniform and the buoyant convection is driven entirely by thermal gradients as reflected in Fig. 2 for B=0.5 T

and b=1. At this time, the maximum value of the streamfunction is 0.00686. In Fig. 3, the hot fluid rises near the periphery of the melt, flows radially inward along the top of the ampoule, axially downward along the centerline of the ampoule, and either solidifies or flows radially outward along the crystal-melt interface. The $O(Ha^{1/2})$ axially upward flow in the parallel layer is reflected in the crowded streamlines adjacent to r=1.

Once crystal growth begins, the crystal-melt interface absorbs silicon and the melt adjacent to the interface is silicon depleted. When 0.25% of the crystal has grown at t=0.9059, the crystal has absorbed some silicon as reflected in the contours of the concentration in the melt in Fig. 4 in which the minimum value of the concentration is 0.636. The silicon-depleted melt has only diffused or convected a short distance from the crystal-melt interface at this early stage of growth and most of the melt remains at the initial concentration C=1. At this early stage, the contours of the concentration are nearly horizontal due to diffusion of the silicon-rich melt towards the interface. The strong axially upward flow adjacent to r=1 has convected the silicon-depleted melt axially upward so that the concentration near the periphery is lower than the concentration near the centerline. The shapes of the streamlines nearly resemble those of Fig. 2. With solutal convection alone, the lighter fluid adjacent to the centerline would rise while the heavier fluid adjacent to the periphery would sink, thus creating a clockwise circulation that opposes the counterclockwise thermal convection. Therefore, the maximum value of the

streamfunction has reduced to 0.00678, which is lower than that for a doped melt in which the melt motion is driven entirely by thermal convection [20].

We present the streamfunction and concentration in the melt at t=72.47 when 20% of the crystal has grown in Figs. 5 and 6, respectively. In Fig. 5, the maximum value of the streamfunction has decreased to 0.000442. In Fig. 6, the minimum and maximum values of the concentration are 0.255 and 1.0, respectively The minimum value of the concentration is small because the segregation coefficient is large. By this stage of growth for a doped crystal, the maximum value of the concentration is C<1 because the thermal convection would have convected the silicon-depleted melt over the entire melt [20]. However, for the present alloyed crystal, the opposing solutal convection has decreased the convective species transport so that a pocket of the melt near r=0 and ζ=+1 still remains at the initial uniform concentration C=1. The axial position corresponding to the maximum value of the streamfunction in Fig. 5 has moved to axially upward. In Fig. 5, there is an opposing circulation adjacent to the crystal-melt interface caused by the concentration gradient.

For most of the remainder of growth, the shapes of the contours of streamfunction and concentration resemble those of Figs. 5 and 6, respectively. The average concentration in the melt continues to decrease as the crystal-melt interface absorbs silicon continuously throughout growth. Near the end of growth, the melt is left totally depleted of silicon because the segregation coefficient is large.

In Fig. 7, we present the contours of the concentration in the crystal. The bottom of the crystal solidified with a relatively radially-uniform composition because the silicon-depleted melt did not have time to convect away. As growth progressed, the contours of the concentration became more curved because the axially-upward flow near r=1 convected the silicon-depleted melt away from the interface. Near the end of growth, the average concentration in the melt is small due to the absorption at the interface. In addition, the compositional variations in the melt are small compared with earlier stages of growth so that the crystal is relatively radially uniform near z=0. The axial composition in the crystal decreases as z increases.

5. Conclusions

We have developed a method to treat buoyant convection and species transport for alloyed crystal growth in a strong magnetic field. We found that the buoyant convection due to compositional variations opposes the buoyant convection due to thermal variations. Thus, the alloyed germanium-silicon crystal solidified with less radial segregation than a doped crystal grown under the same conditions. Because of the large value of the segregation coefficient, the axial variation of the crystal composition is large. Future research will compare asymptotic model predictions to experimental results.

6. Acknowledgements

This research was supported by the National Aeronautics and Space Administration under grant NAG8-1817 and by the U. S. Air Force Office of Scientific Research under grant FA9550-04-1-0249. The calculations were performed on the Cray X1 provided by the DoD High Performance Computing Modernization Program under grant AFSNH2487 and on the IBM P690 provided by the National Science Computational Alliance under grant DMR030015.

7. References

[1] Walker, J. S., Henry, D., and BenHadid H., 2002, "Magnetic stabilization of the buoyant convection in the liquid-encapsulatedCzochralski process," *Journal of Crystal Growth*, Vol, 243, pp. 108-116.

[2] Flemings, M. C., 1974, Solidification Processing, McGraw-Hill.

[3] Khine, Y. Y., Banish, R. M., and Alexander, J. I. D., 2002, "Convective effects during diffusivity measurements in liquids with an applied magnetic field," *International Journal of Thermophysics*, Vol. 23, pp. 649-666.

[4] Watring, D. A., and Lehoczky, S. L., 1996, "Magneto-hydrodynamic Damping of Convection during Vertical Bridgman-Stockbarger Growth of HgCdTe," *Journal of Crystal Growth*, Vol. 167, pp. 478-487.

[5] Ramachandran, N., and Watring, D. A., "Convection Damping by an Axial Magnetic Field during Growth of HgCdTe by Vertical Bridgman Method - Thermal Effects," 35th AIAA Aerospace Sciences Meeting and Exhibit, Paper No. 97-0450, Reno, NV, Jan. 1997.

[6] Alboussiere, T., Moreau, R., and Camel, D., 1991, "Influence of a magnetic field on the solidification of metallic alloys," *Comptes Rendus de l'Academie des Sciences*, Vol. 313, pp. 749-755.

[7] Ma, N., and Walker, J. S., 2000, "A Model of Dopant Transport during Bridgman Crystal Growth with Magnetically damped Buoyant Convection," *Journal of Heat Transfer,* Vol. 122, pp. 159-164.

[8] Hart, J. E., 1971, "On Sideways Diffusive Instability," *Journal of Fluid Mechanics*, Vol. 49, pp. 279-288.

[9] Ma, N., 2003, "Solutal Convection during Growth of Alloyed Semiconductor Crystals in a Magnetic Field," *Journal of Thermophysics and Heat Transfer*, Vol. 17, pp. 77-81.

[10] Ma, N., and Farrell, M. V., 2004, "Macrosegregation during alloyed semiconductor crystal growth in strong axial and transverse magnetic fields," *International Journal of Heat and Mass Transfer*, Vol. 47, pp. 3047-3055.

[11] Liu, Y., Dost, S., Lent, B., and Redden, R. F., 2003, "A three dimensional numerical simulation model for the growth of CdTe single crystals by the traveling heater method under magnetic field," *Journal of Crystal Growth*, Vol. 254, pp. 285-297.

[12] Timchenko, V., Chen, P. Y. P., Leonardi, E., Davis, G. D., and Abbaschian, R., 2002, "A computational study of binary alloy solidification in the MEPHISTO experiment," *International Journal of Heat and Fluid Flow*, Vol. 23, pp. 258-268.

[13] Brailovskaya, V. A., Zilberberg, V. V., and Feoktistova, L. V., 2000, "Numerical investigation of natural and forced solutal convection above the surface of a growing crystal," *Journal of Crystal Growth*, Vol. 210, pp. 767-771.

[14] LeMarec, C., Guerin, R., and Haldenwang, P., 1997, "Pattern study in the 2-D solutal convection above a Bridgman-type solidification front," *Physics of Fluids*, Vol. 9, pp. 3149-3161.

[15] LeMarec, C., Guerin R., and Handenwang, P., 1996, "Radial macrosegregation induced by 3D patterns of solutal convection in upward Bridgman solidification," *Journal of Crystal Growth*, Vol. 169, pp. 147-160.

[16] Garandet, J. P., and Alboussière, T., 1999, "Bridgman Growth: Modelling and Experiments," *The Role of Magnetic Fields in Crystal Growth*, In *Progress in Crystal Growth and Characterization of Materials* (Ed. K. W. Benz), Elsevier Science Publishers, Vol. 38, pp. 73-132.

[17] Walker, J. S., 1999, "Models of Melt Motion, Heat Transfer, and Mass Transport during Crystal Growth with Strong Magnetic Fields," *The Role of Magnetic Fields in Crystal Growth*, In *Progress in Crystal Growth and Characterization of Materials* (Ed. K. W. Benz), Elsevier Science Publishers, Vol. 38, pp. 195-213.

[18] Ma, N., and Walker, J. S., 1997, "Validation of strong magnetic field asymptotic models for dopant transport during semiconductor crystal growth," *Journal of Crystal Growth*, Vol. 180, pp. 401-409.

[19] Ma, N., and Walker, J. S., 2001, "Inertia and Thermal Convection during Crystal Growth with a Magnetic Field," *Journal of Thermophysics and Heat Transfer*, Vol. 15, pp. 50-54.

[20] Ma, N., and Walker, J. S., 2000, "A parametric study of segregation effects during vertical Bridgman crystal growth with an axial magnetic field," *Journal of Crystal Growth*, Vol. 208, pp. 757-771.

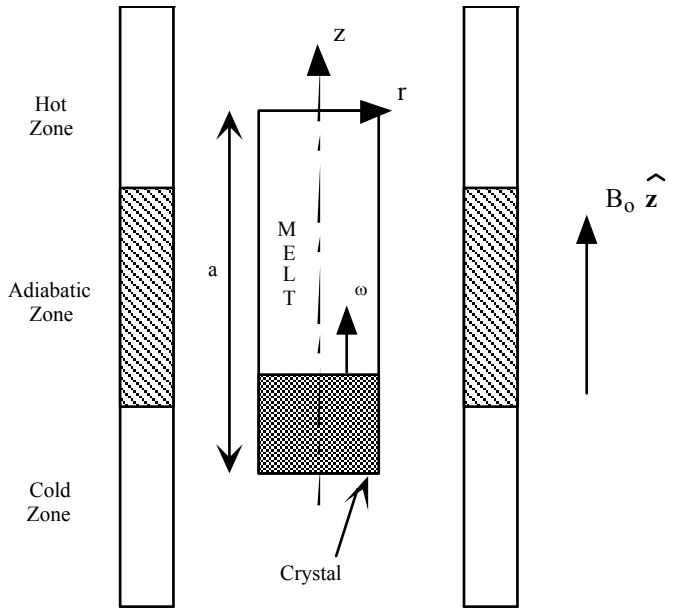

Figure 1: Vertical Bridgman-Stockbarger ampoule with a uniform, steady, axial magnetic field $B\hat{\mathbf{z}}$ and with coordinates normalized by the ampoule's inner radius

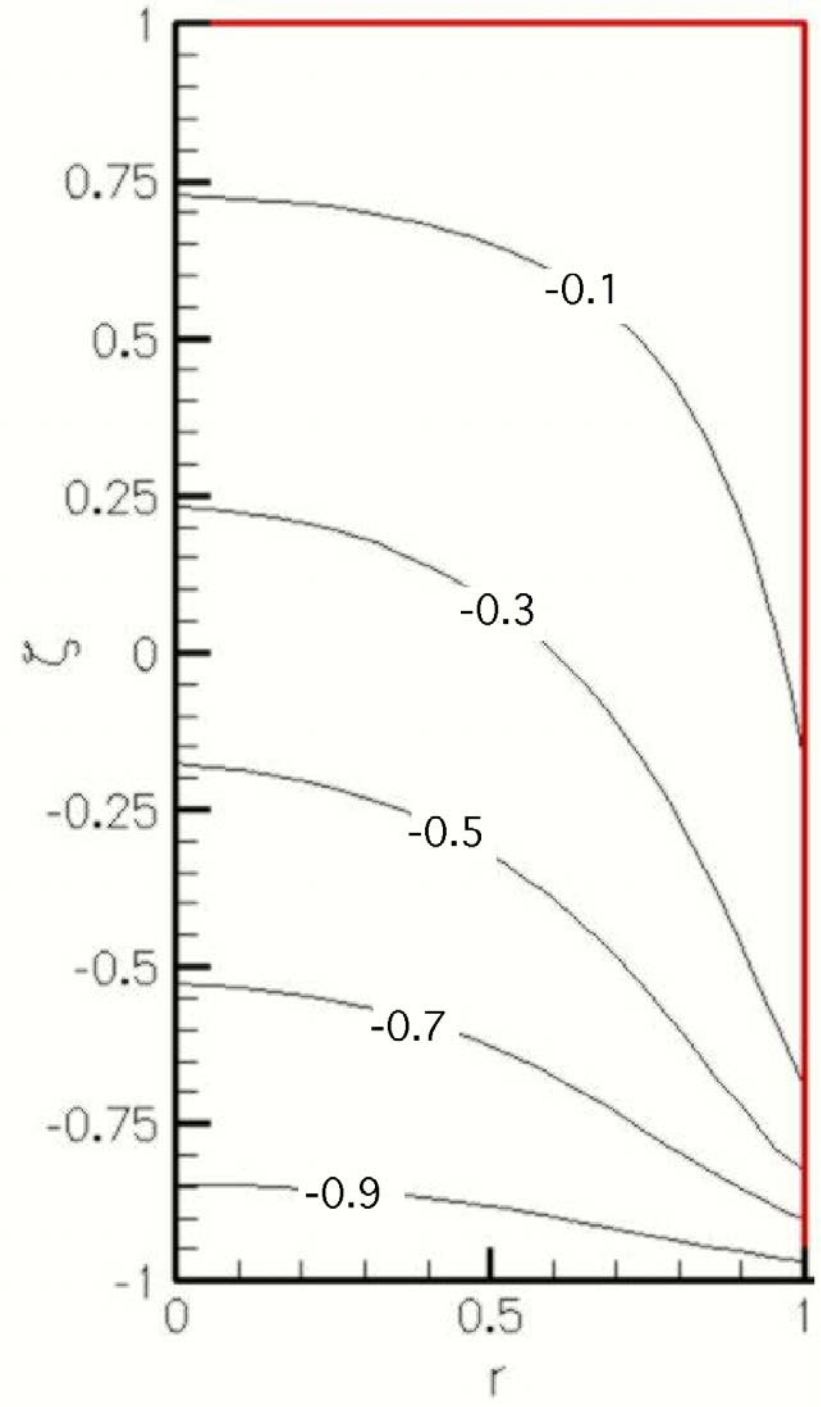

Figure 2: Temperature T(r,ζ,t=0) for Bi=10, d=0.1 and a=1.0.

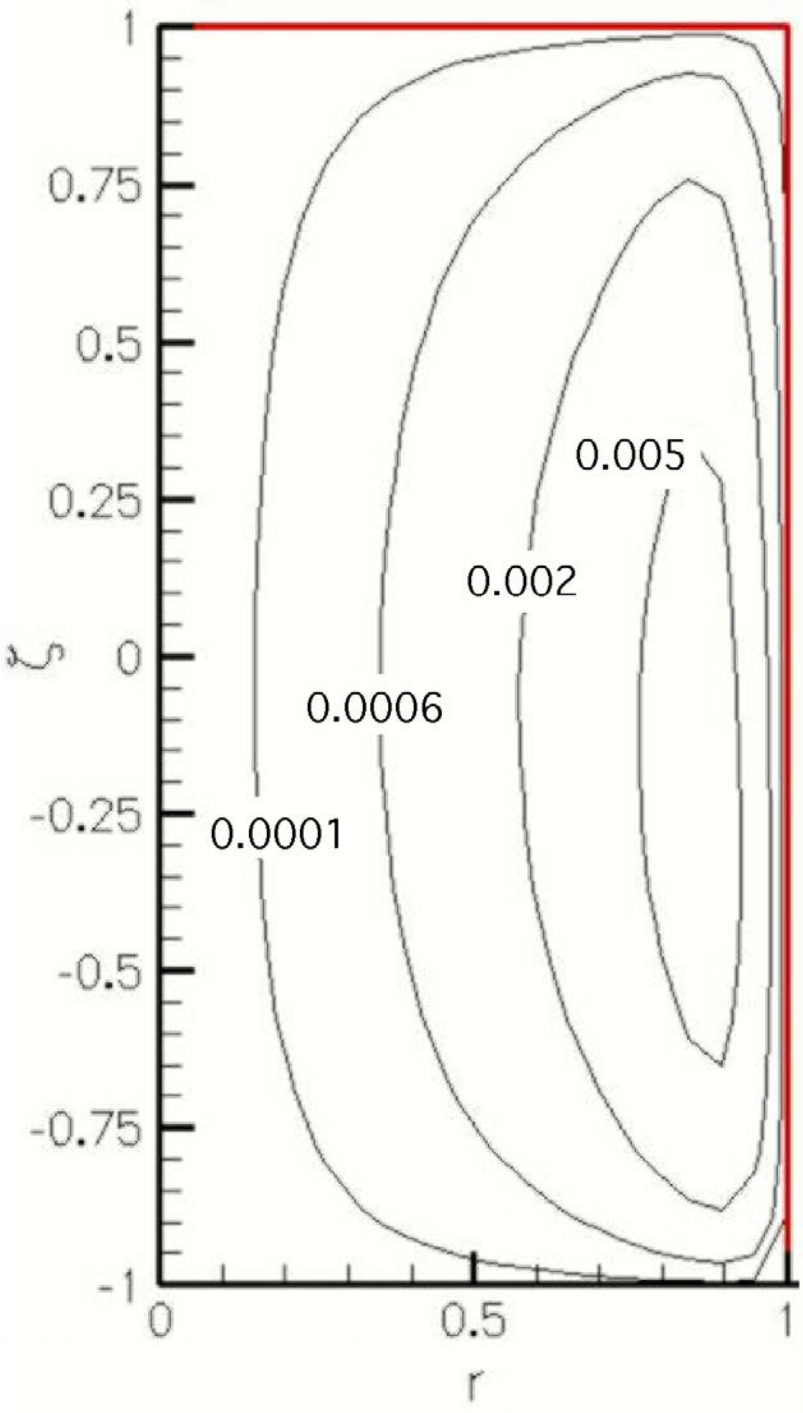

Figure 3: Streamfunction $\psi(r,\zeta,t=0)$ for B=0.5 T and a=1.

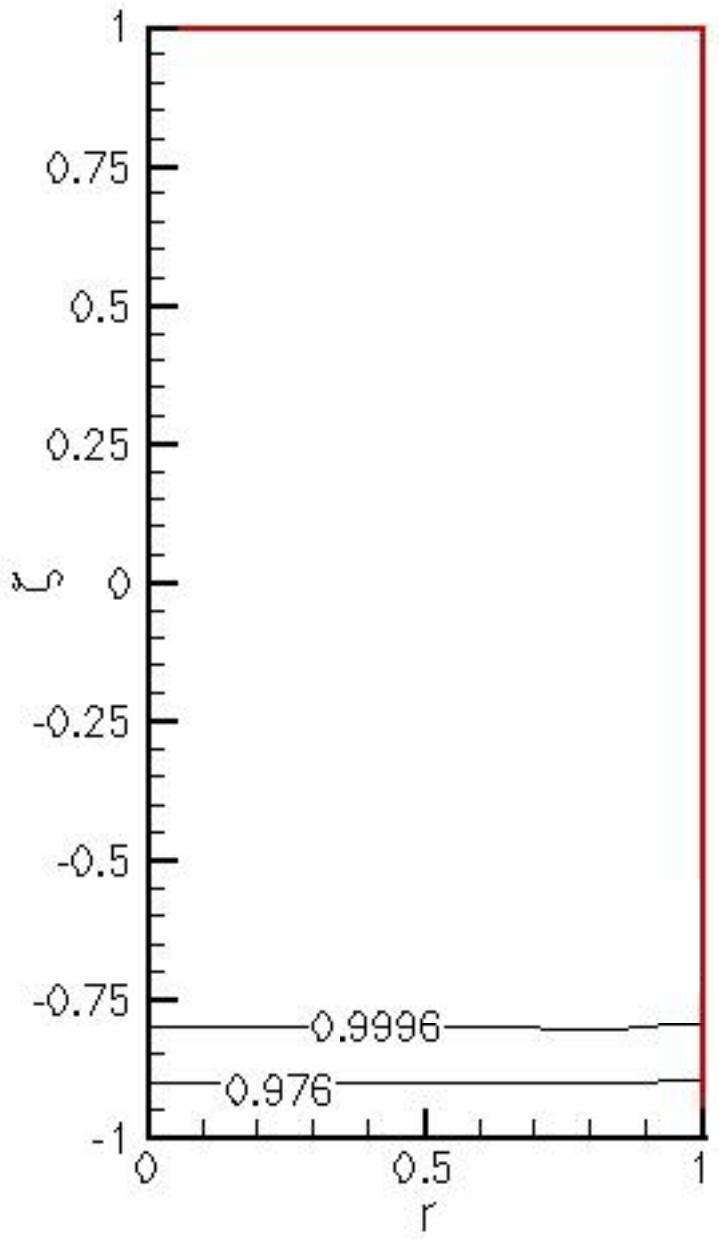

Figure 4: Concentration in the melt C(r,ζ,t=0.9059) for B=0.5 T and C_o=0.10.

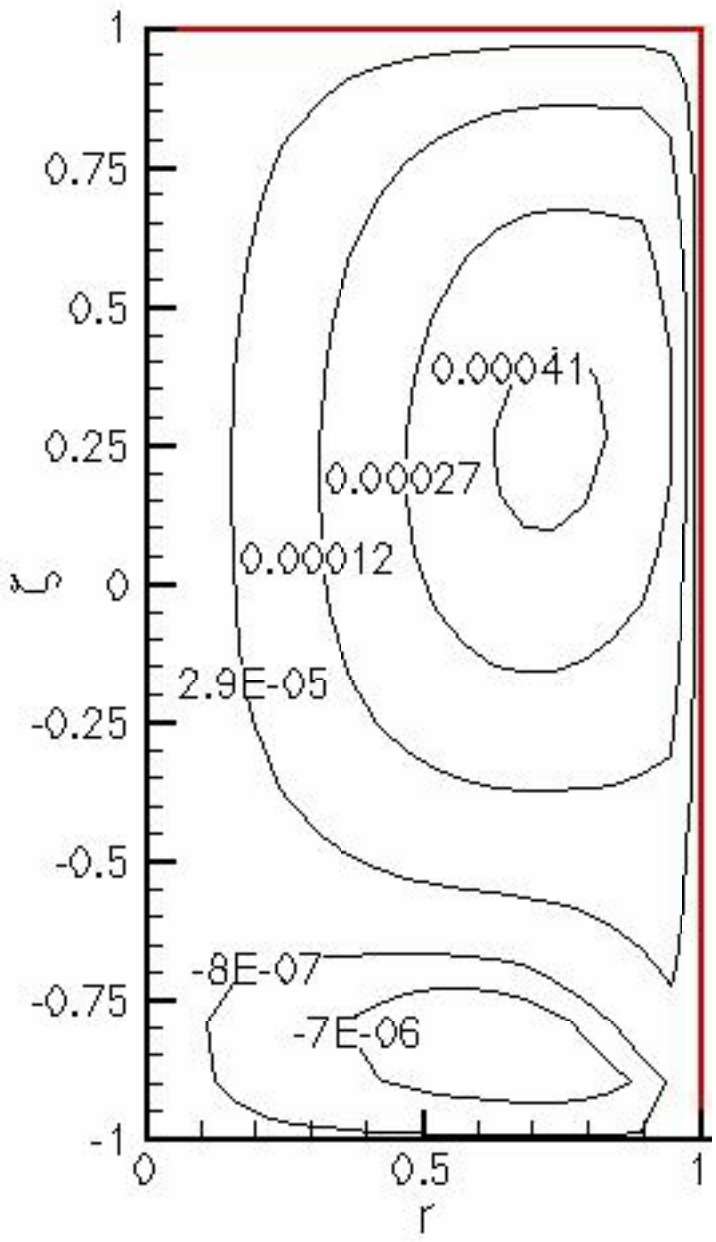

Figure 5: Streamfunction $\psi(r,\zeta,t=72.47)$ for B=0.5 T and C_o=0.10.

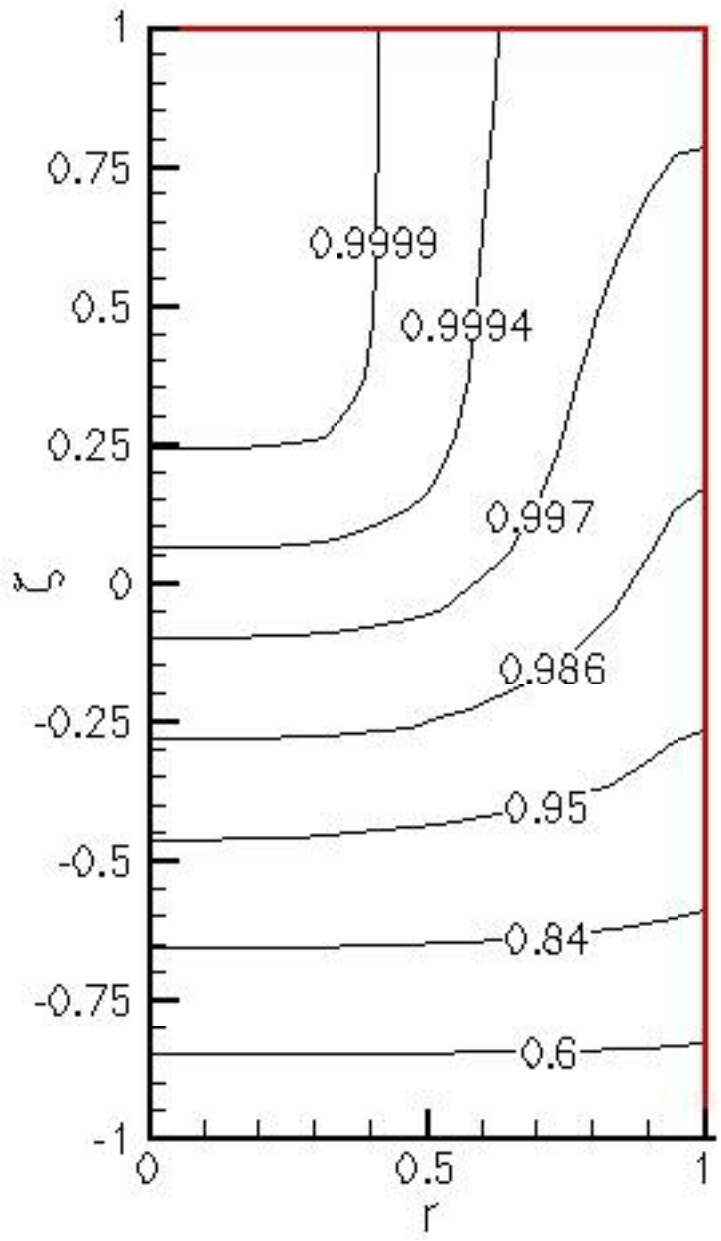

Figure 6: Concentration in the melt C(r,ζ,t=72.47) for B=0.5 T and C_o=0.10.

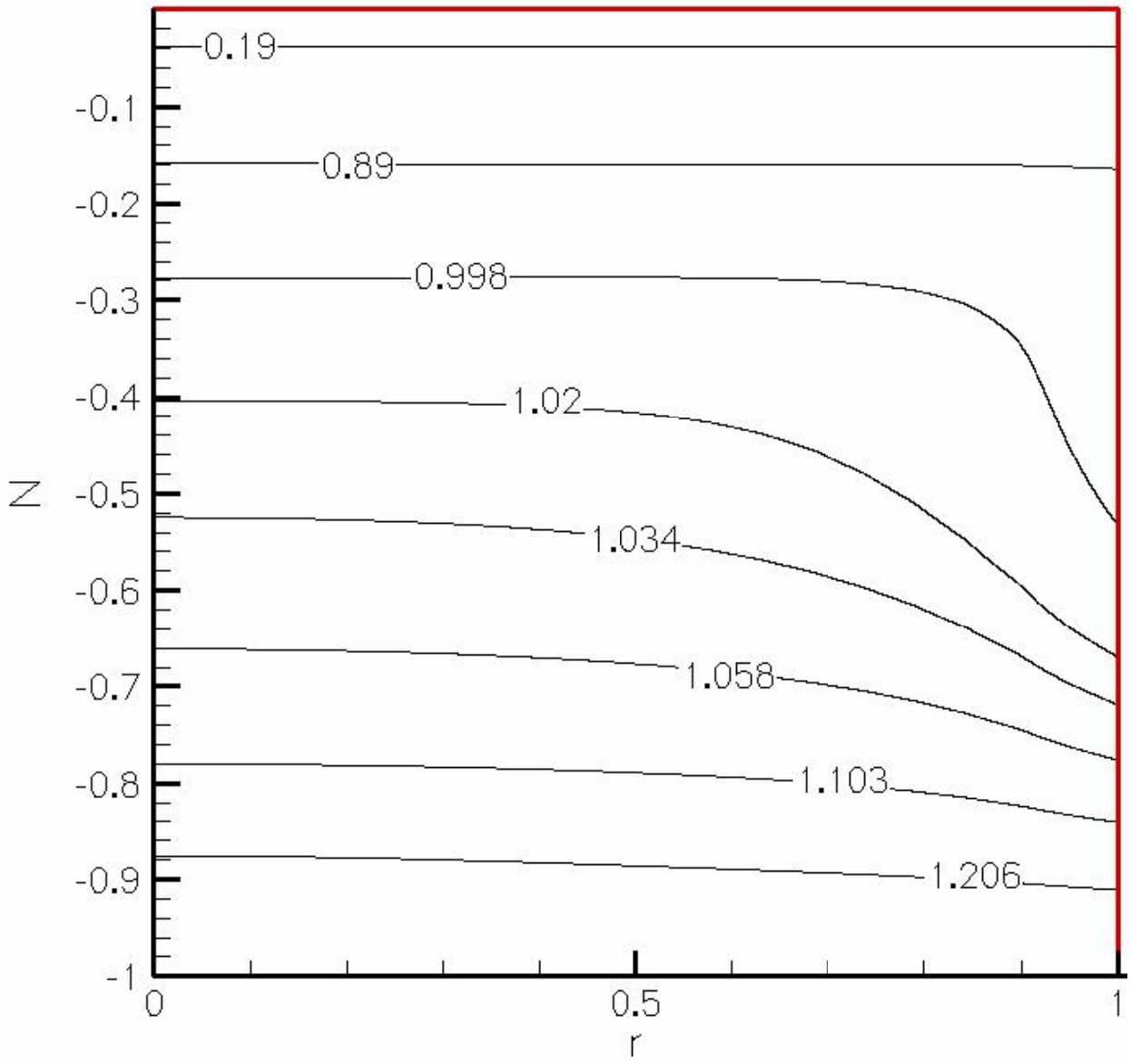

Figure 7: Concentration in the crystal $C_s(r,z)$ for B=0.5 T and C_o=0.10